

First-principles study of the electronic structure, Z_2 invariant and Quantum oscillation in the kagome material CsV_3Sb_5

Shalika R. Bhandari,^{1,2,*} Mohd Zeeshan,³ Vivek Gusain,³ Keshav Shrestha,⁴ and D. P. Rai^{5,†}

¹*Department of Physics, Bhairahawa Multiple Campus, Tribhuvan University, Siddharthanagar-32900, Rupandehi, Nepal*

²*Leibniz Institute for Solid State and Materials Research, IFW Dresden, Dresden-01609, Germany*

³*Department of Physics, Indian Institute of Technology, Hauz Khas, New Delhi-110016, India*

⁴*Department of Chemistry and Physics, West Texas A and M University, Canyon, Texas 79016, USA*

⁵*Department of Physics, Mizoram University, Aizawl 796004, India*

(Dated: October 18, 2024)

This work presents a detailed study of the electronic structure, phonon dispersion, Z_2 invariant calculation, and Fermi surface of the newly discovered kagome superconductor CsV_3Sb_5 , using density functional theory (DFT). The phonon dispersion in the pristine state reveals two negative modes at the M and L points of the Brillouin zone, indicating lattice instability. CsV_3Sb_5 transitions into a structurally stable $2 \times 2 \times 1$ charge density wave (CDW) phase, confirmed by positive phonon modes. The electronic band structure shows several Dirac points near the Fermi level, with a narrow gap opening due to spin-orbit coupling (SOC), though the effect of SOC on other bands is minimal. In the pristine phase, this material exhibits a quasi-2D cylindrical Fermi surface, which undergoes reconstruction in the CDW phase. We calculated quantum oscillation frequencies using Onsager's relation, finding good agreement with experimental results in the CDW phase. To explore the topological properties of CsV_3Sb_5 , we computed the Z_2 invariant in both pristine and CDW phases, resulting in a value of $(\nu_0; \nu_1\nu_2\nu_3) = (1; 000)$, suggesting the strong topological nature of this material. Our detailed analysis of phonon dispersion, electronic bands, Fermi surface mapping, and Z_2 invariant provides insights into the topological properties, CDW order, and unconventional superconductivity in AV_3Sb_5 ($A = \text{K}, \text{Rb}, \text{and Cs}$).

I. INTRODUCTION

In recent years, kagome metals have garnered a significant research interest due to its distinctive quantum characteristics owing to the unique lattice structure resembles to a Japanese bamboo basket. The kagome lattice is composed of a two-dimensional network of corner-sharing triangles and hexagons. A series of layered kagome metals AV_3Sb_5 ($A = \text{K}, \text{Rb}$ and Cs) are found with various intriguing complex properties such as charge density wave (CDW) order, superconductivity (SC), Fermi crossing, band topology with anomalous Hall effect (AHE), flat bands across the Brillouin zone and van Hove singularities (VHSs)¹⁻⁸. These properties originate from the inherent characteristics of the kagome lattice: spin frustration, flat bands, Dirac cones, and VHSs at various locations. So far, the series of AV_3Sb_5 is being synthesized, modeled, and characterized by a number of theoretical⁹⁻¹³ and experimental groups¹⁴⁻²⁰. Our literature survey on Kagome materials indicates that at 80 ~100 K, CDW arises from hexagonal AV_3Sb_5 ($A = \text{K}, \text{Rb}, \text{and Cs}$) compounds with stacked vanadium kagome layers. The CDW phases of AV_3Sb_5 are found to exhibit superconducting behaviour with transition temperature (T_c) = 0.9 ~ 2.5 K^{5,8,21}. With the application of pressure on AV_3Sb_5 , two superconducting domes has been appeared with enhanced T_c and no sign of a structural phase transition²²⁻²⁵. In addition to the translational symmetry breaking in the CDW phase, the rotation and time-reversal symmetry breaking was also appeared on cooling down towards T_c ²⁶⁻²⁸. CDW was re-

cently found in the bilayer kagome metal ScV_6Sn_6 in which the V atoms form kagome bilayers^{21,29} and also in the kagome metal FeGe , that develops antiferromagnetic (AFM) order and results in an improvement of the ordered moment^{30,31}. CDW in kagome metal FeGe offers additional flexibility for studying the interaction between magnetism and CDW. Despite their exceptional similarity, it has been found that the electronic structure of the Cs compound is very different from the K and Rb materials in AV_3Sb_5 ³².

In most studies, the majority of research on the kagome materials are focused on the SC and its relationship to CDW. However, we have observed the limited reports on the topology, Z_2 invariant and Fermi-surface calculations. In the series of AV_3Sb_5 ($A = \text{K}, \text{Rb}$ and Cs), we are particularly interested on CsV_3Sb_5 due to its topologically non-trivial band structure with many Dirac-like band crossing near the Fermi level, highest superconducting T_c and non zero topological invariant Z_2 suggesting a strong candidate for further topological investigation^{24,33-35}.

There are various assumption on the origin of CDW state in AV_3Sb_5 series. Some report that CDW state is induced by the Peierls instability related to the Fermi surface nesting and phonon softening^{36,37}, while other main views on origin of CDW state formation in AV_3Sb_5 series are exciton condensation^{38,39}, momentum-dependent EPC^{40,41}, saddle-point nesting⁴², and Jahn-Teller-like instability⁴³. However, solid knowledge of the lattice and electronic properties for the CDW state is still missing

to understand the superconductivity and topology which calls for future studies. In this study we have presented a first principles electronic calculations on the pristine and CDW states of CsV₃Sb₅, providing a thorough understanding of the experimental work. We report that CDW transition is related to breathing-phonon modes of kagome lattice and mediated by the Fermi surface instability. To confirm the topologically non-trivial band structure, we report Wannier centres on CsV₃Sb₅ for pristine and CDW phase which has been presented for the first time to our knowledge.

II. COMPUTATIONAL DETAILS AND NUMERICAL SOFTWARE

Two computational codes such as WIEN2k⁴⁴ and FPLO (full-potential local-orbital)^{45,46} has been used for the **electronic structure, Z₂ invariant and Fermi surface calculations as reported recently**^{47–49}. Vienna *ab-initio* Simulation Package (VASP) has been used for phonon dispersion calculation by using the finite displacement method(FDM)⁵⁰. We constructed a 3×3×2 (162 atoms) and 2×2×2 (288 atoms) supercell for pristine and ISD structure, respectively, to obtain the phonon dispersion curves using Phonopy package⁵¹. The phonon dispersion curves are obtained by solving the equation,

$$\sum_{\beta\tau'} D_{\tau\tau'}^{\alpha\beta}(\mathbf{q})\gamma_{\mathbf{q}j}^{\beta\tau'} = \omega_{\mathbf{q}j}^2\gamma_{\mathbf{q}j}^{\alpha\tau}. \quad (1)$$

where the indices τ, τ' represent the atoms, α, β are the Cartesian coordinates, \mathbf{q} is a wave vector, j is a band index, $D(\mathbf{q})$ represents the dynamical matrix, ω signifies the corresponding phonon frequency, and γ is the polarization vector.

All the codes are based on the full-potential linearized augmented plane wave method within a frame work of DFT. All-electrons were treated within the standard generalized gradient approximation (PBE-GGA) using the parameterization of Perdew, Burke, and Ernzerhof (PBE-96)⁵². The outermost electron configurations taken for the calculations are 5s²5p⁶6s¹ for Cs, 3s²3p⁶3d³4s² for V, and 4d¹⁰5s²5p³ for Sb, respectively. The electronic bands derived from Cs-5p, V-3d and Sb-5p are fitted to a tight-binding Hamiltonian as in Fig. 4(a) by using the Maximally-Projected Wannier Functions method as implemented in FPLO code to obtain Hamiltonian data (See Fig. 3 in the Supplemental Material for ISD phase). The Wannier fitting was done using pyfplo⁴⁵ module of the FPLO package. The Hamiltonian data were used in the Fermi surface and Z₂ invariant calculations. The four-component Dirac equation was solved for full-relativistic calculations. The first Brillouin zone was integrated within a Bloch corrected linear tetrahedron method using a 12×12×12 **k**-point mesh for the pristine and 18×18×16 **k**-point mesh for CDW state. The self-consistent calculations

were carried out with a spin-orbit coupling (SOC). **We have considered 2×2×1 superlattice for CDW phase calculation due to the presence of weak interlayer interaction.** The Fermi surfaces were generated using 5000 **k**-points which produces a dense **k**- points mesh of 28×28×26. From our DFT calculation, CsV₃Sb₅ is found to be stable with lowest energy in nonmagnetic state and exhibit metallic behaviour, consistent with the experimental report^{1,53}.

III. RESULTS AND DISCUSSION

The crystal structure of CsV₃Sb₅ with the mixture of triangle and layered hexagonal lattices forming the inter-metallic kagome networks^{54,55} as shown in Figs. 1(a) and 1(b). In the 2D Kagome net of V atoms of CsV₃Sb₅, Sb is intercalated by the triangular lattices and Cs atoms at the corner of the cube forming the layered hexagonal-prismatic symmetry with the space group *P6/mmm* (191) as in Figs. 1(a)–1(c). The Kagome net of vanadium is interwoven with a simple hexagonal net made up of Sb1 sites. From a space-filling point of view, the Sb1 atoms fill up the natural gap created in the Kagome plane. Structural optimization of the lattice parameters and atomic positions on experimentally obtained^{1,34} structure was performed until the forces on each atom were less than 0.14 meV/Å. Optimized lattice parameters opted for the calculation are $a= b=5.43$ Å, $c=9.21$ Å, and $\Gamma=120^\circ$. The variation of a and c with the application of pressure for both pristine and ISD phase are presented in Table 1 in Supplemental Material.

A. Phonon Dispersion

The phonon dispersion relations of the pristine and CDW state of CsV₃Sb₅ at ambient pressure has been calculated from the *ab-initio* FDM method and shown in Figs. 1(d)–1(g). In Fig. 1(d), **we have found two negative energies of the soft acoustic phonon modes (two imaginary phonon frequencies) at the first Brillouin zone around M and L points.** This finding is consistent with the previous reports^{56–58} and indicates a strong instability. Such instability plays an important role to drive the CDW transition. The structural instabilities led by these soft modes, the Star of David (SoD) and tri-hexagonal (TrH) (also named the inverse Star of David (ISD)) structure configurations are proposed to be the likely candidates for CDW structures. In Fig. 1(d), the L-point soft mode suggests the presence of a 2×2×2 reconstruction, whereas the M-point soft mode is associated with a breathing phonon of V atoms in the kagome lattice. Both the the symmetry points have the same in-plane projection which is equivalent to the vector of the CDW order. Moving to 2×2 supercell ISD structure, the imaginary frequencies disappear in the phonon band spectra

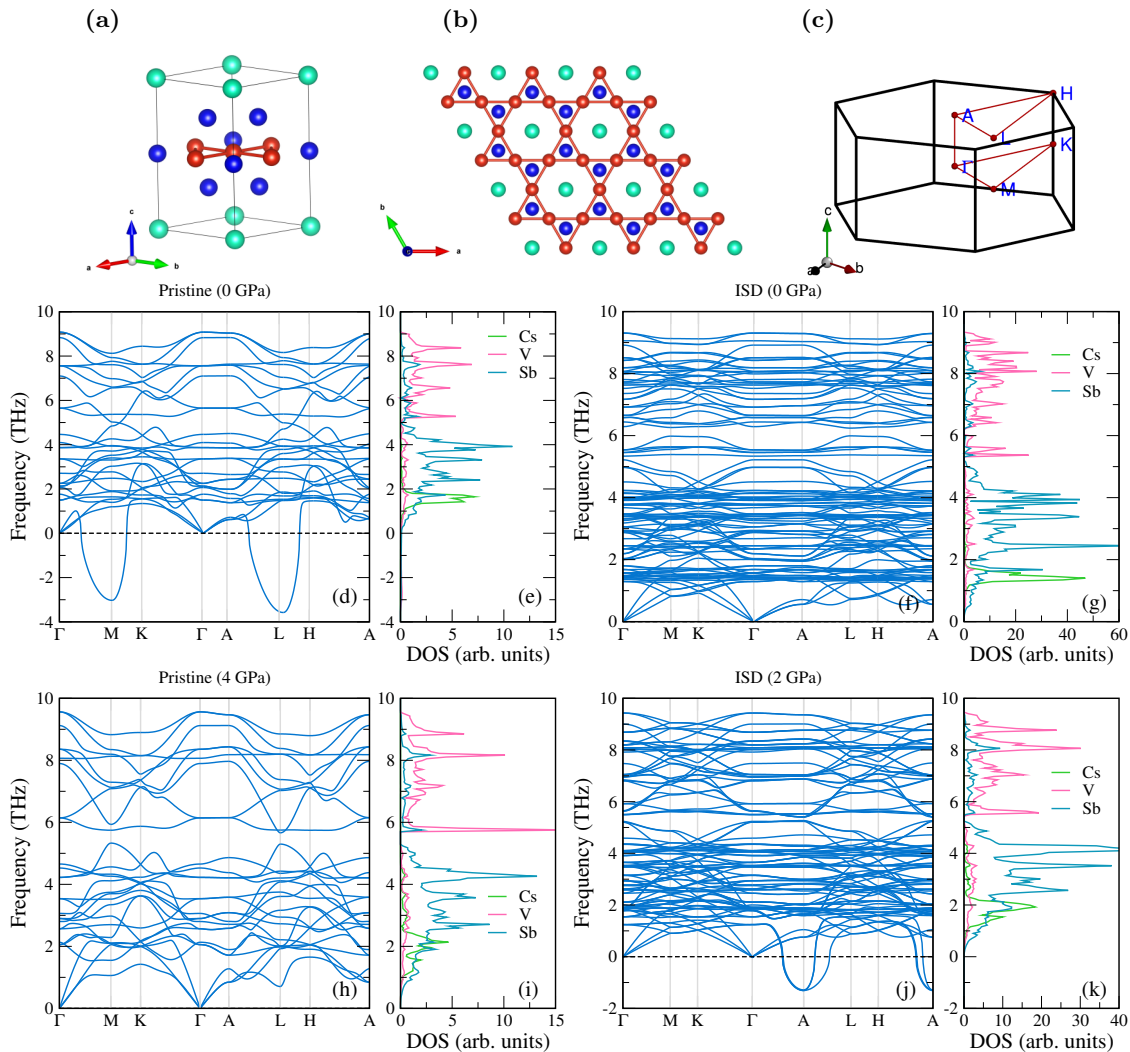


FIG. 1. (a) A unit cell of CsV_3Sb_5 . (b) Top view of CsV_3Sb_5 layer showing kagome layer of V atoms. Atom represented by cyan, red, and blue denote Cs, V and Sb, respectively. (c) Brillouin zone of the space group $P6/mmm$ (191) and the main symmetry directions. (d) Phonon dispersions bands structure and density of states of pristine phase of CsV_3Sb_5 at 0 GPa. Imaginary (negative) phonon frequency in (d) corresponds to the breathing mode of the kagome lattice. Such a breathing instability is related to CDW distortions. Breathing out and breathing in lead to two different structure in CDW phase. (f) Phonon dispersions band structure and density of states of $2 \times 2 \times 2$ ISD state of CsV_3Sb_5 at 0 GPa. (g) Phonon dispersions band structure and density of states of $2 \times 2 \times 2$ pristine state of CsV_3Sb_5 at 4 GPa. (j) Phonon dispersions band structure and density of states of $2 \times 2 \times 2$ ISD state of CsV_3Sb_5 at 2 GPa.

as in Fig. 1(f). The ISD structure forms by an inverse deformation when V1 (V2) atoms move away (toward) the center, which is comparable to the well-known CDW effect in 1T TaS_2 ⁵⁹. Breathing in and out lead to two distinct structures and breathing deformation reduces the total energy, hence ISD structure achieve the dynamically stable structure.

For the confirmation of its stability on ground state, we also checked the ground state energies of SD and ISD structure. On comparing the ground state energies, we found that, in the $2 \times 2 \times 2$ CDW, the SD phase has higher energy in its ground state and relaxes to the ISD structure spontaneously. A recent study on the stability of

CDW surface by using a slab model have also shown that the ISD phase is more stable with the Cs termination^{5,60}. Therefore, the ISD structure is energetically favored than the SD.

We have also studied the pressure effect on phonon dispersion for low range pressure upto 6 GPa for both pristine and CDW phase. Phonon dispersion for both state for 1–6 GPa has been presented in supplementary materials (Fig. 1 and Fig. 2 in the Supplemental Material). For pristine phase, the imaginary phonon modes at M and L points gradually decreases upto 3 GPa and it completely vanishes at and above 4 GPa (Fig. 1 in the Supplemental Material). It shows complete suppression of CDW phase

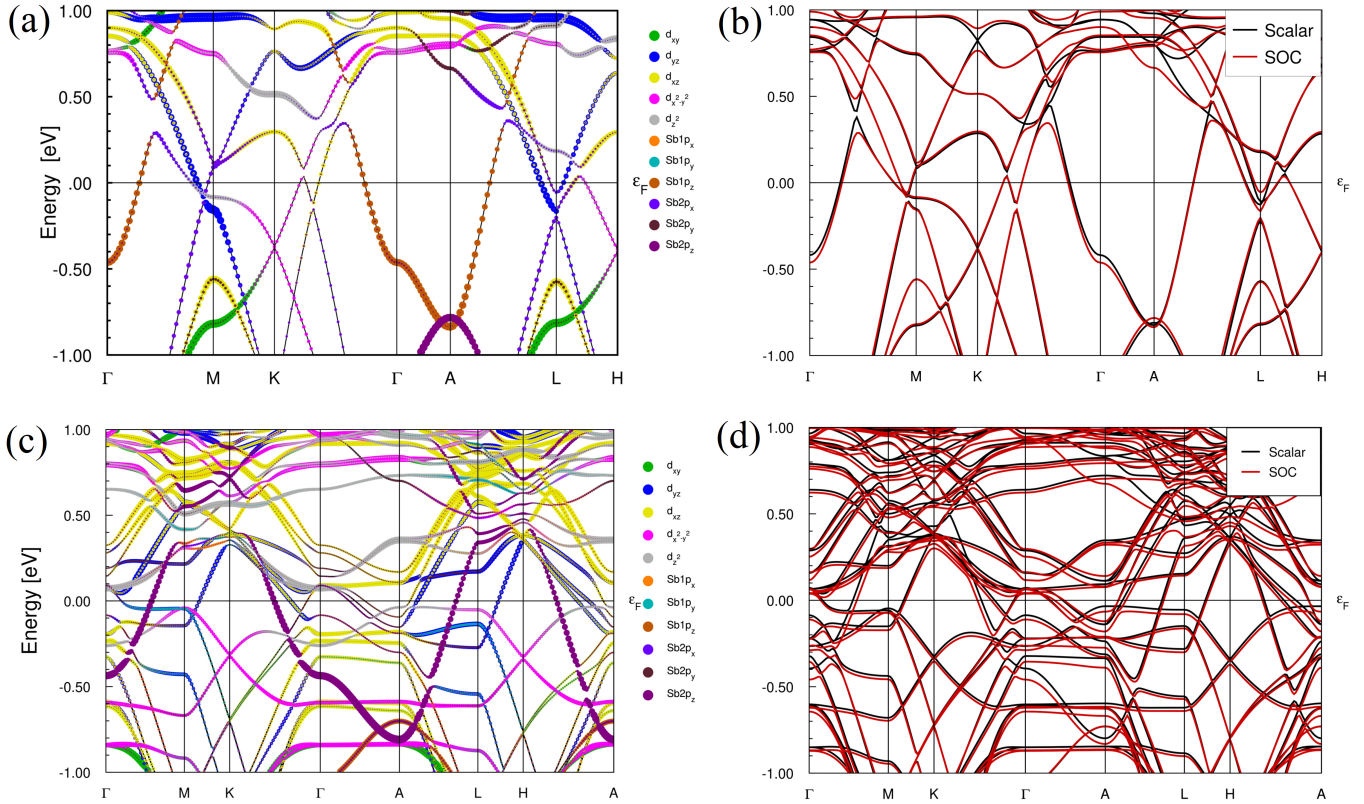


FIG. 2. DFT calculated (a) Orbital resolved electronic band structure of Pristine phase, (b) Electronic band structure of Pristine phase CsV_3Sb_5 with and without SOC, (c) Orbital resolved electronic band structure of $2 \times 2 \times 1$ CDW phase, (d) Electronic band structure of $2 \times 2 \times 1$ CDW phase.

with increasing pressure which agrees with earlier experimental report⁶¹. In case of CDW state, interestingly imaginary phonon modes appear at 2 GPa and it vanishes at and above 3 GPa (Fig. 2 in the Supplemental Material). The imaginary phonon at 2 GPa is supposed to be due to the structural distortion which mainly consist of movement of V atoms in the ab plane. Some studies propose electronic correlations at ambient pressure and CDW fluctuations around 2 GPa to be the main driving force behind the formation of Cooper pairs^{12,62,63}. This imaginary phonon modes in CDW phase also predicts the suppression of CDW phase at 2 GPa which needs further experimental examination.

B. Crystal, Electronic structure and Fermi surface

The CDW state is found to be three dimensional (3D) and be modulated along the c -axis. This modulation, which is still in debate, is either $2 \times 2 \times 2$ or $2 \times 2 \times 4$ for AV_3Sb_5 series with $2 \times 2 \times 2$ reported for KV_3Sb_5 and both $2 \times 2 \times 2$ and $2 \times 2 \times 4$ reported for CsV_3Sb_5 ^{64–66}. The $2 \times 2 \times 2$ CDW has similar electronic structure as the $2 \times 2 \times 1$ one, because of the weak interlayer interaction⁵⁸. For simplicity of analysis and computational capacity, we

focus only on the in-plane distortion, $2 \times 2 \times 1$ superlattice (i.e., 2×2) CDW phase in the following discussions.

The total and partial density of states (DOS) (See Fig. 3 in the Supplemental Material) and orbital-resolved band structure of CsV_3Sb_5 for pristine and CDW phase within GGA+SOC are shown in Fig. 2. The major contribution to the total DOS around E_F is mainly from V-3d and Sb-5p orbitals. Here, Fermi surface lies within vanadium d -orbital. The DOS exhibits a local minima near E_F , indication of a semi-metal. The calculated orbital-resolved band structure of normal-state CsV_3Sb_5 shows that there are two bands (band 67 and 68) crossing the E_F . The two bands that cross the E_F around the Γ and A points are primarily provided by the out-of-plane orbitals of Sb- p_z , and the bands near the M and L points are dominated by the out-of-plane orbitals of V- d_{xz}/d_{yz} . Additionally, we detect several Dirac points close to the E_F , that are dominated by the in-plane orbitals of V- $d_{xy}/d_{x^2-y^2}$ [Fig. 2(b)], agreeing well with previous DFT report^{6,58}. Aside from a set of dispersive bands around Γ and A, the majority of band crossings are caused by Dirac-like features at H, K, L and even at H-A. A fascinating aspect of the band diagram can be found if we look the features at K and H points. These are not isolated Dirac cones; when we look at the dispersion along K-H,

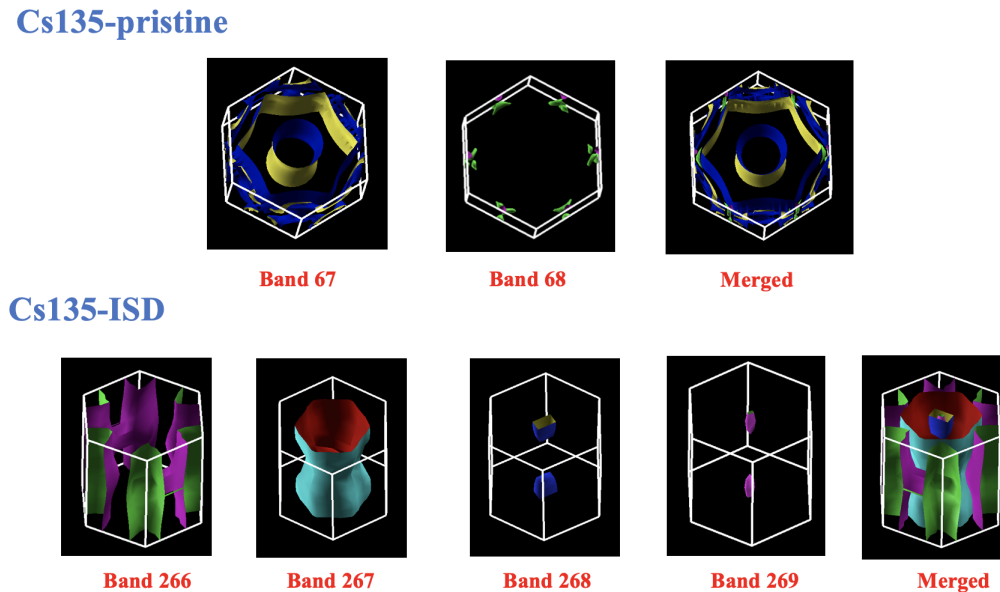


FIG. 3. Band-resolved DFT computed Fermi-surfaces of the pristine and $2 \times 2 \times 1$ CDW phases of CsV_3Sb_5 . A strong 2D characteristic is seen which has cylinder-shaped Fermi surface centered near Γ and the large hexagonal Fermi surface in its vicinity in pristine phase. The significant reconstruction due to distortion is obtained in the Fermi-surface sheet of the CDW phase. The Fermi surface from all bands is displayed in the final picture in both.

it has been found that the features are linked together, developing a conical valley. The strength of the related inter-layer coupling influences the bulk band structure: In CsV_3Sb_5 the interlayer coupling is found to be weak resulting in a quasi two-dimensional (2D) band structure. In the band structure, four VHSs points formed by Vanadium $3d$ orbitals around the M point near to the E_F are identified which are in agreement with earlier work^{1,2,25,32,67}. Three of them are near to the E_F and another is just below the E_F around M point. VHSs with their large density of states that bring to a significant decrease of the local Coulomb interaction and also plays an important role for the different Fermi surface instabilities which is supported by ARPES experiment^{32,67}.

A comparison of band structure in the pristine and charge density wave (CDW) state are shown in Figs. 2(c) and 2(f), respectively. The general characteristics of band in CDW state, which has large number of bands due to supercell structure, are unchanged for those **which are contributed from Sb-orbitals near Γ points. Dirac cones at K and H points of BZ below E_F remain unbroken in both state [Figs. 2(c) and 2(f)], which are consistent with earlier report⁵.** The bands near BZ which are contributed by V orbitals have been changed in CDW state and with application of SOC which can be seen at M and L symmetry points. It is due to $2 \times 2 \times 1$ distortion on V kagome lattice and effect of SOC in $3d$ orbitals. These characters can be rationalized by the fact that bands close to the E_F are mostly contributed by V. It has been found from the calculation that SOC affects some of the Sb- p bands, and it also opens a small gap at the Dirac point near K [Fig. 2 (c)], but it does not alter the location

of the VHSs points which are in agreement with previous work⁶⁸. Here, we investigate that both pristine and CDW state has a topologically nontrivial band structure with non zero Z_2 topological invariant for the band near E_F [see detail in section C]. From DFT calculations the topological invariant Z_2 for CsV_3Sb_5 is found to be $(\nu_0; \nu_1\nu_2\nu_3) = (1; 000)$. This suggests to a π -Berry phase accumulated along the cyclotron orbit which is consistent with cylindrical shape Fermi surface as in Fig. 3.

The Fermi surface (FS) of CsV_3Sb_5 Kagome compound for pristine and ISD phase from the relevant band structures has been presented in Fig. 3. Both electron and hole-like sheets has been found in the topology which has an important contribution while identifying the sign of the Hall coefficient of a material⁶⁹. In the pristine state, a cylinder-like FS is centered around the Γ -point (or along the Γ -A path) for band 67 contributed by Sb- Pz states, suggesting a 2D nature of the electronic properties. A big and complex electron/hole-like hexagonal sheet (FSS) contributed by V- d states centered around the Γ -point is also obtained. A much smaller FSS hole-like and electron-like FS sheet is appeared along the Γ -M path and near K-points respectively, that are contributed by V- d states, for band 68.

On the other hand, the 2×2 ISD CDW distortion modifies the FSSs. The Fermi surface becomes reconstructed by the CDW pattern. The bands near the BZ boundary at M and K are strongly modified, including the large hexagonal FS and small FSSs. Different from V- d driven FSSs, the cylinderlike FSSs from Sb- Pz is marginally affected by the CDW deformation, as shown in Fig. 3. Because the breathing distortion mainly involve

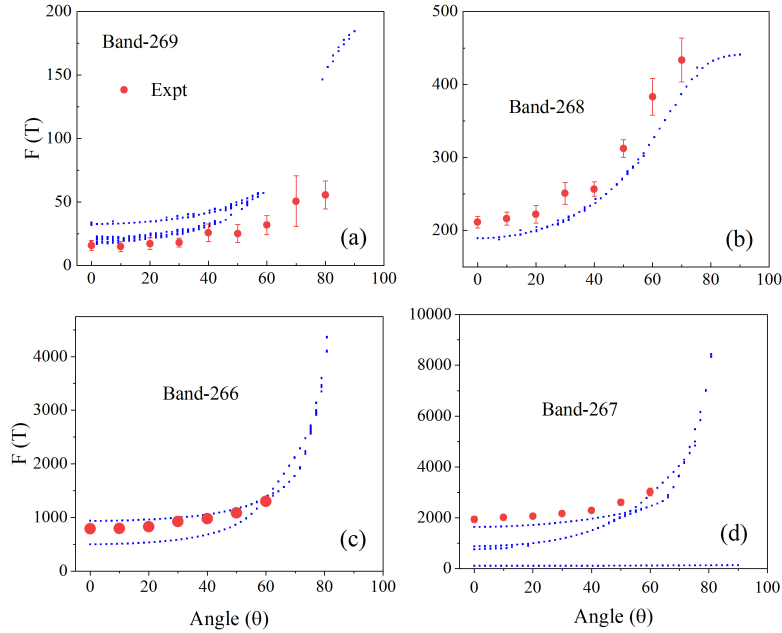


FIG. 4. Comparison between theoretically calculated frequencies with the experimental values at different angles. Theoretical values are calculated using the SKEAF code and experimental values are adapted from the reference⁸. Theoretical values are in good agreement with the experimental frequencies.

the V kagome lattice, the CDW and electron lattice interaction are band selective. Our results regarding the electronic band structure and the Fermi surface are in good agreement with earlier report^{1,5}.

In Fig. 4, we present a comparison between the experimental and calculated angular dependences of the Fermi surface (FS) area for CsV₃Sb₅. The experimental data are adapted from the reference⁸. The Onsager relationship⁷⁰ was used to convert the theoretical Fermi surface cross-sectional areas into oscillatory frequencies for comparison with the experimental values. As seen from the graph, the theoretically calculated frequencies are in good agreement with the experimental data.

C. Z_2 Invariant calculation

Topological behavior of the materials are called strong or weak based on four Z_2 topological invariants ($\nu_0; \nu_1\nu_2\nu_3$) which is proposed by Fu-Kane⁷¹⁻⁷³. If $\nu_0 = 1$, and other indices ($\nu_1\nu_2\nu_3$) are equal to zero, the material is classified with strong topological material; if $\nu_0 = 0$ and any of the indices ($\nu_1\nu_2\nu_3$) is equal to one, it is a weak topological material. In the former case, the time reversal symmetry (TRS)-protected surface states are present on all facets, while in the latter case, such surface states are present only on certain facets. The bands that change the Z_2 -invariant from trivial to non-trivial or vice versa we call topologically active bands, whereas the ones that do not change Z_2 are called topologically inactive bands. Formally topological activity can be calcu-

lated separately for all (even crossing) bands. The change in topological nature, however, only manifests itself in a warped or real gap above the last active band. For the pristine and ISD structure model of CsV₃Sb₅, Z_2 invariants were calculated through Fu Kane indices⁷². This computation was carried out directly from the PW92 band structure with resorting to an approximate Wannier representation. DFT calculations were done with FPLO code using the GGA in the PW92 parametrization. The self-consistent calculations were carried out with spin-orbit coupling (SOC) included. The band structure of the pristine and CDW phase also displays non-trivial band inversion^{1,2}. For both cases, we calculate the Z_2 topological invariants and found that both pristine and CDW phase with $(\nu_0; \nu_1\nu_2\nu_3) = (1; 000)$ which is consistent with previous reports^{1,2,58}. Hence, the compound CsV₃Sb₅ is categorized to be rich with strong topological behavior providing clear evidence of nontrivial topological band structures.

We confirmed the automatized calculation of these invariants by visual inspection of the Wannier centres as shown in Fig. 5(b). These Wannier centres on CsV₃Sb₅ for pristine and CDW phase has been presented for the first time to our knoweldge. A clean straight reference line can be drawn for θ Fig. 5(b)., which only crosses this center and hence crosses an odd number of Wannier centers, which results in $Z_2 = 1$. This and the fact that we can visually connect the Wannier center curves in a reasonable smooth way convinces us that the topological indices are 1;(000). For trivial cases, there will be a region around θ where reference line passes without crossing or even number of curves cross in Wannier centre curves.

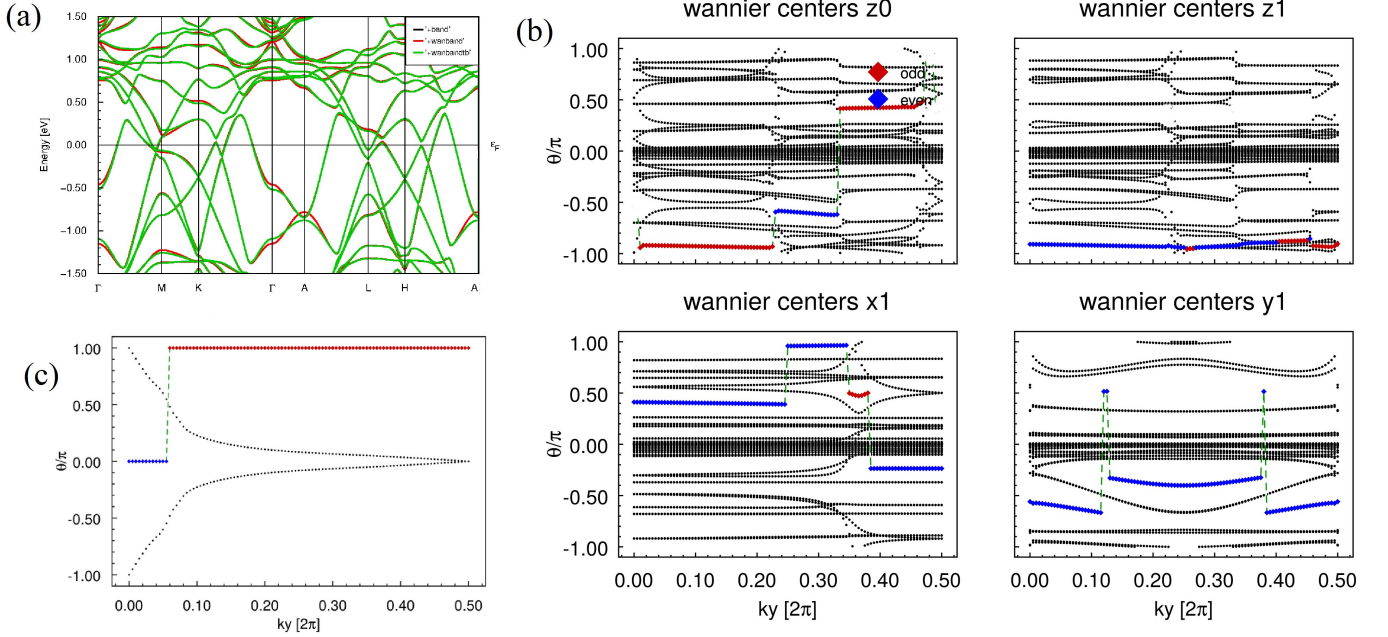


FIG. 5. (a) Wannier model bands (red/green) fitted from fpo. (b) Non trivial Z_2 invariant Wannier center curve representation in the plane spanned by the TRIM. (c) Wannier centers and reference line for homo 67. The x_1, y_1 and z_1 planes have zero Z_2 invariant, while plane z_0 is non-trivial.

Hence we get 0;(000).

The Wannier centers and reference line for homo 67 for pristine phase of CsV_3Sb_5 are presented in Fig. 5(b) (See Fig. 5 in the Supplemental Material for ISD phase). Here, Wannier centers where the last suffix indicates in which plane we are: z_0 is a $(1/2 \ 1/2 \ 0)$ plane through the origin in primitive reciprocal basis, while x_1, y_1 and z_1 denote $(0 \ 1/2 \ 1/2)$, $(1/2 \ 0 \ 1/2)$ and $(0 \ 1/2 \ 1/2)$ planes through $(1/2 \ 0 \ 0)$, $(0 \ 1/2 \ 0)$ and $(0 \ 0 \ 1/2)$.

It can be clearly seen that the x_1, y_1 and z_1 planes have a region ($\theta = 0.5$ or else) where a reference line can pass without any centers crossing in Fig. 5(b), which indicates trivial nature, while for the z_0 -plane an odd number of curves cross any reference line (see Fig. 5 (c) for reference), which indicates plane z_0 is non-trivial. We also confirm this by algorithm which we use which has been set as the reference line is printed with blue weights if the number of centers crossed so far is even and in red weights if the number is odd. If the last data point is odd the invariant is non-trivial. [A version of this algorithm⁷⁴ is linked directly into FPLO.](#) At the end we call the invariant odd if a majority of these gap-following curves indicate oddness as can be seen in Fig. 5.

IV. SUMMARY

By means of density functional calculations, we studied pressure effect for low range pressure on phonon dispersion for both pristine and CDW phase of CsV_3Sb_5 . We found that the calculated phonon dispersion relations on

the pristine state of CsV_3Sb_5 at ambient pressure shows two negative energies of the soft acoustic phonon modes at the first Brillouin zone around M and L points consistent with the previous reports. This structural instability is the cause for 2×2 reconstruction and CDW phase. Interestingly, imaginary phonons are appeared in CDW phase at 2 GPa due to structural distortion which suggest the suppression of CDW phase. We have also carried out DFT calculations for electronic structure and Fermi surfaces. A strong 2D characteristic is seen which has cylinder-shaped Fermi surface centered near Γ and the large hexagonal Fermi surface in its vicinity in pristine phase. Our DFT calculations confirmed that the Fermi surface of CsV_3Sb_5 reconstructs in the CDW phase. From Fu-Kane indices and a version of algorithm linked directly into FPLO, we calculated Z_2 invariants for both state of CsV_3Sb_5 . For both cases, we calculate the Z_2 topological invariants and found that both pristine and CDW phase with $(\nu_0; \nu_1\nu_2\nu_3) = (1; 000)$ which is consistent with previous reports. We also confirmed the nontrivial topological band structures by presenting with Wannier centres curves. The detailed Fermi surface and Z_2 invariants information for CsV_3Sb_5 and the corresponding DFT calculations reported here will be essential to comprehending the superconductivity, charge density wave, and topological phase in CsV_3Sb_5 and other AV_3Sb_5 family members.

ACKNOWLEDGEMENTS

SRB and DPR thanks DST, India for ISRF research fellowship (Award No. INSA/DST-ISRF/2022/35).

Computations were performed using HPC at IFW Dresden, Germany. We thank Ulrike Nitzsche for technical assistance.

* Shalika Ram Bhandari:shalikram.bhandari@bmc.tu.edu.np
 † D. P. Rai:dibyaprakashrai@gmail.com

REFERENCES

- ¹ B. R. Ortiz, L. C. Gomes, J. R. Morey, M. Winiarski, M. Bordelon, J. S. Mangum, I. W. H. Oswald, J. A. Rodriguez-Rivera, J. R. Neilson, S. D. Wilson, E. Ertekin, T. M. McQueen, and E. S. Toberer, *Phys. Rev. Mater.* **3**, 094407 (2019).
- ² B. R. Ortiz, S. M. L. Teicher, Y. Hu, J. L. Zuo, P. M. Sarte, E. C. Schueller, A. M. M. Abeykoon, M. J. Krogstad, S. Rosenkranz, R. Osborn, R. Seshadri, L. Balents, J. He, and S. D. Wilson, *Phys. Rev. Lett.* **125**, 247002 (2020).
- ³ R. Chapai, M. Leroux, V. Oliviero, D. Vignolles, M. P. Smylie, D. Y. Chung, M. G. Kanatzidis, W.-K. Kwok, J. F. Mitchell, and U. Welp, *Phys. Rev. Lett.* **130**, 126401 (2023).
- ⁴ K. Shrestha, V. Marinova, D. Graf, B. Lorenz, and C. W. Chu, *Phys. Rev. B* **95**, 075102 (2017).
- ⁵ H. Tan, Y. Liu, Z. Wang, and B. Yan, *Phys. Rev. Lett.* **127**, 046401 (2021).
- ⁶ M. Kang, S. Fang, J. K. Kim, B. R. Ortiz, S. H. Ryu, J. Kim, J. Yoo, G. Sangiovanni, D. D. Sante, B. G. Park, C. Jozwiak, A. Bostwick, E. Rotenberg, E. Kaxiras, S. D. Wilson, J. H. Park, and R. Comin, *Nat. Phys.* **18**, 301 (2022).
- ⁷ S. Ni, S. Ma, Y. Zhang, J. Yuan, H. Yang, Z. Lu, N. Wang, J. Sun, Z. Zhao, D. Li, S. Liu, H. Zhang, H. Chen, K. Jin, J. Cheng, L. Yu, F. Zhou, X. Dong, J. Hu, H.-J. Gao, et al., *Chin. Phys. Lett.* **38**, 057403 (2021).
- ⁸ K. Shrestha, R. Chapai, B. K. Pokharel, D. Miertschin, T. Nguyen, X. Zhou, D. Y. Chung, M. G. Kanatzidis, J. F. Mitchell, U. Welp, D. Popovi, D. E. Graf, B. Lorenz, and W. K. Kwok, *Phys. Rev. B* **105**, 024508 (2022).
- ⁹ Y.-P. Lin and R. M. Nandkishore, *Phys. Rev. B* **104**, 045122 (2021).
- ¹⁰ C. Setty, H. Hu, L. Chen, and Q. Si, arXiv:2105.15204.
- ¹¹ T. Park, M. Ye, and L. Balents, *Phys. Rev. B* **104**, 035142 (2021).
- ¹² X. Wu, T. Schwemmer, T. Müller, A. Consiglio, G. Sangiovanni, D. Di Sante, Y. Iqbal, W. Hanke, A. P. Schnyder, M. M. Denner, M. H. Fischer, T. Neupert, and R. Thomale, *Phys. Rev. Lett.* **127**, 177001 (2021).
- ¹³ J. Zhao, W. Wu, Y. Wang, and S. A. Yang, *Phys. Rev. B* **103**, L241117 (2021).
- ¹⁴ E. Uykur, B. R. Ortiz, O. Iakutkina, M. Wenzel, S. D. Wilson, M. Dressel, and A. A. Tsirlin, *Phys. Rev. B* **104**, 045130 (2021).
- ¹⁵ F. H. Yu, D. H. Ma, W. Z. Zhuo, S. Q. Liu, X. K. Wen, B. Lei, J. J. Ying, and X. H. Chen, *Nat. Commun.* **12**, 3645 (2021).
- ¹⁶ K. Y. Chen, N. N. Wang, Q. W. Yin, Y. H. Gu, K. Jiang, Z. J. Tu, C. S. Gong, Y. Uwatoko, J. P. Sun, H. C. Lei et al., *Phys. Rev. Lett.* **126**, 247001 (2021).
- ¹⁷ T. Nguyen, N. Aryal, B. K. Pokharel, L. Harnagea, D. Miertschin, D. Popovi, D. E. Graf, and K. Shrestha, *Phys. Rev. B* **106**, 075154 (2022).
- ¹⁸ K. Shrestha, M. Shi, B. Regmi, T. Nguyen, D. Miertschin, K. Fan, L. Z. Deng, N. Aryal, S.-G. Kim, D. E. Graf, X. Chen, and C. W. Chu, *Phys. Rev. B* **107**, 155128 (2023).
- ¹⁹ K. Shrestha, D. Miertschin, R. Sankar, B. Lorenz, and C. W. Chu, *Journal of Physics: Condensed Matter* **33**, 335501 (2021).
- ²⁰ B. R. Ortiz, P. M. Sarte, E. M. Kenney, M. J. Graf, S. M. L. Teicher, R. Seshadri, and S. D. Wilson, *Phys. Rev. Mater.* **5**, 034801 (2021).
- ²¹ H.W.S. Arachchige, W. R. Meier, M. Marshall, T. Mat-suoka, R. Xue, M. A. McGuire, R. P. Hermann, H. Cao, and D. Mandrus, *Phys. Rev. Lett.* **129**, 216402 (2022).
- ²² N. N. Wang, K. Y. Chen, Q. W. Yin, Y. N. N. Ma, B. Y. Pan, X. Yang, X. Y. Ji, S. L. Wu, P. F. Shan, S. X. Xu et al., *Phys. Rev. Research* **3**, 043018 (2021).
- ²³ F. Du, S. Luo, B. R. Ortiz, Y. Chen, W. Duan, D. Zhang, X. Lu, S. D. Wilson, Y. Song, and H. Yuan, *Phys. Rev. B* **103**, L220504 (2021).
- ²⁴ Z. Liang, X. Hou, F. Zhang, W. Ma, P. Wu, Z. Zhang, F. Yu, J.-J. Ying, K. Jiang, L. Shan, Z. Wang, and X.-H. Chen, *Phys. Rev. X* **11**, 031026 (2021).
- ²⁵ A. A. Tsirlin, P. Fertey, B. R. Ortiz, B. Klis, V. Merkl, M. Dressel, S. D. Wilson, and E. Uykur, arXiv:2105.01397.
- ²⁶ H. Chen, et al. *Nature* **559**, 228 (2021).
- ²⁷ H. Li, et al. *Nat. Phys.* **18**, 270 (2022).
- ²⁸ Y.-X. Jiang, et al. *Nat. Mater.* **20**, 1357 (2021).
- ²⁹ S. Cao, C. Xu, H. Fukui, et al. *Nat Commun* **14**, 7671 (2023).
- ³⁰ X. Teng, L. Chen, F. Ye, E. Rosenberg, Z. Liu, J.-X. Yin, Y.-X. Jiang, J. S. Oh, M. Z. Hasan, K. J. Neubauer, B. Gao, Y. Xie, M. Hashimoto, D. Lu, C. Jozwiak, A. Bostwick, E. Rotenberg, R. J. Birgeneau, J.-H. Chu, M. Yi, and P. Dai, *Nature* **609**, 490 (2022).
- ³¹ J.-X. Yin, Y.-X. Jiang, X. Teng, M. S. Hossain, S. Mardanya, T.-R. Chang, Z. Ye, G. Xu, M. M. Denner, T. Neupert, B. Lienhard, H.-B. Deng, C. Setty, Q. Si, G. Chang, Z. Guguchia, B. Gao, N. Shumiya, Q. Zhang, T. A. Cochran, D. Multer, M. Yi, P. Dai, and M. Z. Hasan, *Phys. Rev. Lett.* **129**, 166401 (2022).
- ³² H. LaBollita and A. S. Botana *Phys. Rev. B* **104**, 205129 (2021).
- ³³ L. Nie, K. Sun, W. Ma, D. Song, L. Zheng, Z. Liang, P. Wu, F. Yu, J. Li, M. Shan, D. Zhao, S. Li, B. Kang, Z. Wu, Y. Zhou, K. Liu, Z. Xiang, J. Ying, Z. Wang, T. Wu, and X. Chen, *Nature (London)* **604**, 59 (2022).
- ³⁴ B. R. Ortiz, P. M. Sarte, E. M. Kenney, M. J. Graf, S. M. L. Teicher, R. Seshadri, and S. D. Wilson, *Phys. Rev. Mater.* **5**, 034801 (2021).
- ³⁵ M. M. III, D. Das, J.-X. Yin, H. Liu, R. Gupta, Y.-X. Jiang, M. Medarde, X. Wu, H. C. Lei, J. Chang, P. Dai, Q. Si, H. Miao, R. Thomale, T. Neupert, Y. Shi, R. Khasanov, M. Z. Hasan, H. Luetkens, and Z. Guguchi, *Nature (London)* **602**, 245 (2022).

- ³⁶ R. E. Peierls, *Quantum theory of solid* (Clarendon Press, Oxford, 1996)
- ³⁷ W. Kohn, Phys. Rev. Lett. **2**, 393 (1959).
- ³⁸ C. Chen, B. Singh, H. Lin, and V. M. Pereira, Phys. Rev. Lett. **121**, 226602 (2018).
- ³⁹ J. van Wezel, P. Nahai-Williamson, and S. S. Saxena, Phys. Rev. B **81**, 165109 (2010).
- ⁴⁰ M. D. Johannes and I. I. Mazin, Phys. Rev. B **77**, 165135 (2008).
- ⁴¹ A. Y. Liu, Phys. Rev. B **79**, 220515(R) (2009).
- ⁴² X. Zhou, Y. Li, X. Fan, J. Hao, Y. Dai, Z. Wang, Y. Yao, and H.-H. Wen, Phys. Rev. B **104**, L041101 (2021).
- ⁴³ C. Wang, S. Liu, H. Jeon, and J.-H. Cho, arXiv:2109.01921.
- ⁴⁴ P. Blaha, K. Schwarz, G. K. H. Madsen, D. Kvasnicka, and J. Luitz, (*Technische Universität Wien, Vienna, Austria, 2001*), ISBN 3-9501031-1-2.
- ⁴⁵ K. Koepf and H. Eschrig, Phys. Rev. B **59**, 1743 (1999).
- ⁴⁶ <https://www.FPLO.de>.
- ⁴⁷ B. Mali, H. S. Nair, T. Heitmann, H. Nhalil, D. Antonio, K. Gofryk, S. R. Bhandari, M. P. Ghimire, S. Elizabeth Phys. Rev. B, **102**, 014418 (2020).
- ⁴⁸ S. R. Bhandari, D.K. Yadav, B.P. Belbase, M Zeeshan, B Sadhukhan, D.P. Rai, R.K. Thapa, G.C. Kaphle, M. P. Ghimire. RSC Adv. **10**, 16179?16186 (2020).
- ⁴⁹ D. Miertschin, T. Nguyen, S. R. Bhandari, K. Shtefienko, C. Phillips, B. A. Magar, R. Sankar, D. E. Graf, K. Shrestha. Phys. Rev. B, **110**, 085140 (2024).
- ⁵⁰ G. Kresse and J. Furthmüller, Phys. Rev. B **54**, 11169 (1996).
- ⁵¹ A. Togo and I. Tanaka, Scr. Mater. **108**, 5 (2015).
- ⁵² J. P. Perdew, K. Burke, and M. Ernzerhof, Phys. Rev. Lett. **77**, 3865 (1996).
- ⁵³ E. M. Kenney, B. R. Ortiz, C. Wang, S. D. Wilson, and M. Graf, J. Phys. Condens. Matter **33**, 235801 (2021).
- ⁵⁴ Y.-X. Jiang, J.-X. Yin, M. M. Denner, N. Shumiya, B. R. Ortiz, J. He, X. Liu, S. S. Zhang, G. Chang, I. Belopolski et al., Nat. Mater. **20**, 1353 (2021).
- ⁵⁵ H. Zhao, H. Li, B. R. Ortiz, S. M. Teicher, T. Park, M. Ye, Z. Wang, L. Balents, S. D. Wilson, and I. Zeljkovic, Cascade of Correlated Electron States in a Kagome Superconductor CsV₃Sb₅, arXiv:2103.03118.
- ⁵⁶ Jian-Feng Zhan, Kai Liu and Zhong- Yi Lu, Phys. Rev. B. **104** 195130 (2021).
- ⁵⁷ Jian-Guo Si, Wen-Jian Lu, Yu-Ping Sun, Peng-Fei Liu and Bao-Tian Wang, Phys. Rev. B., **105**, 024517 (2022).
- ⁵⁸ H. Tan, Y. Liu, Z. Wang, and B. Yan, Phys. Rev. Lett. **127**, 046401 (2021).
- ⁵⁹ J. A. Wilson, F. J. Di Salvo, and S. Mahajan, Adv. Phys. **24**, 117 (1975).
- ⁶⁰ H. Chen et al., Roton pair density wave and unconventional strong-coupling superconductivity in a topological kagome metal, arXiv:2103.09188.
- ⁶¹ Z. Zhang, Z. Chen, Y. Zhou, Y. Yuan, s. wang, J. Wang, H. Yang, C. An, L. Zhang, X. Zhu, Y. Zhou, and Z. yang, Phys. Rev. B **103**, 224531 (2021).
- ⁶² T. Neupert, M. M. Denner, J.-X. Yin, R. Thomale, and M. Z. Hasan, Nat. Phys. **18**, 137 (2022).
- ⁶³ M. Wenzel, A.A. Tsirlin, F. Capitani, et al. npj Quantum Mater. **8**, 45 (2023).
- ⁶⁴ Jiang YX, Yin JX and Denner MM et al. Nat. Mater. **20**, 1353 (2021).
- ⁶⁵ Li H, Zhang TT and Yilmaz T et al. Phys. Rev. X **11**, 031050 (2021).
- ⁶⁶ Nakayama K, Li Y and Kato T et al. Phys. Rev. B **104**, L161112 (2021).
- ⁶⁷ Y. Hu, X. Wu, B. R. Ortiz, S. Ju, X. Han, J. N. C. Plumb, M. Radovic, R. Thomale, S. D. Wilson, A. P. Schnyder and M. Shi, Nat. Commun. **13**, 2220 (2022).
- ⁶⁸ K. Nakayama, Y. Li, M. Liu, Z. Wang, T. Takahashi, Y. Yao, and T. Sato, Phys. Rev. B **104**, L161112 (2021).
- ⁶⁹ M.I. Naher, F. Parvin, A.K.M.A. Islam, S.H. Naqib, Eur. Phys. J. B **91**, 289 (2018).
- ⁷⁰ D. Shoenberg, Magnetic Oscillations in Metals (Cambridge University Press, Cambridge, 1984).
- ⁷¹ C. L. Kane and E. J. Mele, Phys. Rev. Lett. **95**, 226801 (2005).
- ⁷² L. Fu, and C. L. Kane, Phys. Rev. B, **76**, 045302 (2007).
- ⁷³ D. J. Thouless, M. Kohmoto, M. P. Nightingale, and M. den Nijs, Phys. Rev. Lett. **49**, 405 (1982).
- ⁷⁴ A. A. Soluyanov, Phys. Rev. B **83**, 235401 (2011).
- ⁷⁵ S.-Y. Yang, Y. Wang, B. R. Ortiz, D. Liu, J. Gayles, E. Derunova, R. Gonzalez-Hernandez, L. Šmejkal, Y. Chen, S. S. P. Parkin, S. D. Wilson, E. S. Toberer, T. McQueen, and M. N Ali, Sci. Adv. **6**, 6003 (2020).
- ⁷⁶ Q. Yin, Z. Tu, C. Gong, Y. Fu, S. Yan, and H. Lei, Chin. Phys. Lett. **38**, 037403 (2021).
- ⁷⁷ Yu.-X. Jiang et al., Discovery of topological charge order in kagome superconductor KV₃Sb₅, arXiv:2012.15709.
- ⁷⁸ Y. Fu, N. Zhao, Z. Chen, Q. Yin, Z. Tu, C. Gong, C. Xi, X. Zhu, Y. Sun, K. Liu, and H. Lei, Phys. Rev. Lett. **127**, 207002 (2021).
- ⁷⁹ Y. Singh, D. Pal, S. Ramakrishnan, A. M. Awasthi, and S. K. Malik, Phys. Rev. B **71**, 045109 (2005).